

Wet granular bed eroded by a dry granular flow

Lama Braysh,^{1,*} Patrick Mutabaruka,^{2,†} Farhang Radjai,^{1,‡} and Serge Mora^{1,§}

¹*LMGC, University of Montpellier, CNRS, France*

²*Geo-Ocean, Univ. Brest, CNRS, IFREMER, Plouzané, France*

(Dated: March 3, 2026)

Using three-dimensional Discrete Element Method (DEM) simulations, we investigate the erosion dynamics of a cohesive bed composed of wet spherical particles subjected to the shear flow of an overlying non-cohesive granular layer. Cohesion is modeled through a capillary attraction law, where the erosion process is governed by the irreversible rupture of liquid bridges at the interface. By systematically varying the liquid-vapor surface tension and the inclination angle of the bed, we analyze the influence of cohesive strength and flow intensity on the mass entrainment rate. Our results identify two distinct erosion regimes: a slow, stochastic regime driven by granular temperature fluctuations, and a fast, collective regime characterized by a global mechanical instability of the interface. We propose a robust scaling law for the surface erosion rate in the fast erosion regime, based on the interplay between two dimensionless parameters: the inertial number (I) and the cohesion index (ξ). This framework reveals that the threshold for the fast erosion regime is determined by the ratio of the geometric mean of the driving stresses (kinetic and pressure) to the cohesive resistance. These findings provide a comprehensive description of the coupling between inertial and capillary forces, offering a predictive tool for the stability of cohesive interfaces in sheared granular flows.

Keywords: Erosion; Cohesion; Numerical simulations; Discrete Element Method; Pendular regime; Granular material

PACS numbers:

I. INTRODUCTION

The mechanical behavior of granular materials is significantly altered by the presence of cohesive forces. In unsaturated wet granular systems, for instance, the addition of a small amount of liquid induces cohesive interactions between the particles due to the surface tension of the liquid, enabling the formation of solid-like structures such as sandcastles [1, 2]. These liquid bonds also generate lubrication forces due to the liquid viscosity [3, 4]. From a rheological perspective, a homogeneous unsaturated wet granular material is characterized by its cohesive strength σ_c , which represents the maximum tensile stress the capillary bonds can sustain. The flow behavior and the resulting microstructure also depend on the confining pressure σ_p , which accounts for the external or lithostatic forces [5], as well as the kinetic stress σ_k . This latter, defined as $\sigma_k = \rho d^2 \dot{\gamma}^2$, arises from the collective motion of particles and depends on the shear rate $\dot{\gamma}$, the particle density ρ , and the particle diameter d [6, 7].

The rheology of homogeneous wet granular materials has been extensively studied both experimentally [8, 9] and numerically [10–12]. It is now well established that at least three dimensionless numbers govern the physics of these systems. The inertial number I represents the interplay between particle inertia and confining stress,

defined as [7, 13–18]

$$I = \sqrt{\sigma_k / \sigma_p}. \quad (1)$$

Experimental and numerical studies show that the apparent friction coefficient μ and packing fraction Φ of steady flows of dry granular materials are unique functions of I [13, 14, 19, 20]. The other dimensionless parameters accounting for capillary cohesion and viscosity are the cohesion index [3, 16, 17, 21]

$$\xi = \sigma_c / \sigma_p \quad (2)$$

and the Stokes number

$$St = \sigma_k / \sigma_v, \quad (3)$$

where σ_v relates to viscous stresses [8, 22, 23]. Recent studies have shown that when inertial, cohesive, and viscous forces are simultaneously present, the system can be described by a combined visco-cohesive inertial number [24–27].

The erosion of a cohesive granular material by a fluid or dry particle flow is of great importance in nature and industrial applications. A relevant example is the evolution of wet agglomerates embedded in a flow of non-cohesive granular materials [3, 28, 29]. In these contexts, an equilibrium is often reached between the cohesive forces maintaining the aggregate and the erosive action of non-cohesive particles. In industrial mixers or rotating drums, this motion is generated by the container's rotation, whereas in geophysics, it is driven by gravity. For instance, during a landslide, debris flows down a slope and erodes the underlying soil, which is often a cohesive

*Electronic address: lama.braysh@umontpellier.fr

†Electronic address: patrick.mutabaruka@ifremer.fr

‡Electronic address: franck.radjai@umontpellier.fr

§Electronic address: serge.mora@umontpellier.fr

granular medium [30, 31]. While the erosion of a granular bed by a liquid has been extensively modeled by transport models [32, 33], our understanding of erosion caused by a granular flow remains much more limited. In such cases, particles at the interface can be irreversibly detached wherever capillary bonds are broken [3, 4, 34, 35].

In this work, we use simulations to investigate a bed of wet, cohesive particles overlaid by a shear flow of non-cohesive dry particles on an inclined plane (see Fig. 1). When the inclination angle θ exceeds the avalanche angle of the dry layer but remains below the critical threshold required for the cohesive bed to flow, the system reaches a metastable state where the dry layer flows over a static cohesive substrate. The resulting erosion is a purely interfacial phenomenon, governed by the competition between the shear stress exerted by the dry flow and the stabilizing effects of cohesion σ_c and confining pressure σ_p .

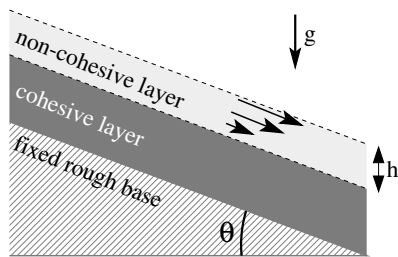


FIG. 1: Schematic representation of the system, consisting of two granular layers deposited on a rough, rigid plane inclined at an angle θ relative to the horizontal, within a vertical gravitational field g . The upper layer comprises a non-cohesive granular medium in a flow state driven by gravity. The underlying layer consists of a cohesive granular medium, initially at rest. The erosion process occurs at the interface between these two distinct phases, where particles are detached from the cohesive bed and entrained into the overlying dry flow.

As in the rheology of wet granular flows, the erosion dynamics at the interface between a cohesive bed or wet agglomerate and a flowing dry particles can in principle be described in terms of the dimensionless numbers I , ξ , and St . However, there are two fundamental differences between these two problems. First, the rheology of a cohesive granular material is a bulk behavior whereas erosion dynamics occurs at the interface between two media. Secondly, in rheology of cohesive flows the inertial and cohesive effects are simultaneously present everywhere inside the flow while for erosion the effects of attraction forces and viscous forces only play a role within the cohesive layer, controlling the cohesive strength against the shear flow, and the inertial effects concern only non-cohesive particles in the dry layer. For these reasons, we expect a nontrivial scaling behavior of the erosion rate with respect to system parameters.

In this article, we examine how the erosion process evolves as a function of key system parameters, including the dry layer thickness, the inclination angle, and the magnitude of the cohesive forces. We operate under con-

ditions where the viscous stress (σ_v) remains negligible in comparison to the other governing stresses. This assumption allows us to isolate the competition between inertial and capillary forces without the complexity of lubrication effects. We demonstrate the existence of two distinct erosion regimes separated by a critical inclination angle θ_c . For $\theta < \theta_c$, the erosion occurs on a grain-by-grain basis driven by rare, intermittent stochastic events; this is referred to as the “slow erosion regime”. Conversely, for $\theta > \theta_c$, the system enters a “fast erosion regime”, triggered when the static equilibrium conditions of the cohesive bed are no longer satisfied, leading to a massive entrainment of particles.

The article is organized as follows. In Section II, we detail the physical processes leading to the two aforementioned erosion regimes. This theoretical framework allows us to derive a scaling law for the critical angle θ_c and to identify the characteristic timescales involved in the fast erosion regime. In Section III, we present the numerical method based on Discrete Element Method (DEM) simulations used to investigate the erosion of a cohesive bed by a non-cohesive flow on an inclined plane. Section IV presents the simulation results, focusing specifically on the fast erosion regime. We establish a scaling law for the surface erosion rate, providing a unified framework for predicting mass entrainment in cohesive granular systems within this regime. Finally, Section V provides a concluding discussion and outlines future perspectives for this work.

II. THEORETICAL FRAMEWORK

In this section, we develop a theoretical analysis of the erosion process to derive the governing laws for the fractional entrainment rate (K_e). We distinguish between the stochastic mechanisms prevalent at low stresses and the collective mechanical instability occurring at higher shear rates. These analytical derivations provide the scaling foundations that will be compared against the results of DEM simulations presented in Section IV.

A. Stability Analysis

In the mechanical description of granular systems, the resistance to deformation is characterized by the ratio of the shear stress σ_τ to the normal stress σ_n . The static friction coefficient μ_s represents the maximum stress ratio that a granular medium can sustain before yielding. The criterion for stability is given by $\sigma_\tau \leq \mu_s \sigma_n$, where μ_s defines the threshold required to initiate flow from a state of rest. The dynamic friction coefficient μ characterizes the medium once it is in a state of flow. In this case, the stress ratio σ_τ/σ_n is no longer a constant threshold but depends on the flow conditions (notably the shear rate).

While μ_s defines the stability of dry grains, the presence of inter-particle bonds in a cohesive bed enhances this resistance. Following recent developments in wet granular flows [24], the static threshold μ_c of the cohesive bed can be expressed as:

$$\mu_c = \mu_s(1 + a\xi), \quad (4)$$

where a is a material-dependent constant and ξ is the cohesion index. In granular rheology, a distinction exists between μ_s and the quasi-static limit μ_0 (the limit of the effective friction as the flow velocity tends toward zero). While μ_s is typically slightly larger than μ_0 due to grain interlocking at rest, for the sake of simplicity and as a first-order approximation, we hereafter assume $\mu_s \simeq \mu_0$.

The cohesive strength σ_c within the bed arises from capillary bridge forces:

$$\sigma_c \sim \frac{2\pi\gamma_s \cos(\Theta_\ell)}{d}, \quad (5)$$

where γ_s is the surface tension and Θ_ℓ is the liquid-solid contact angle. By normalizing this strength by the confining pressure σ_p exerted by the overlying dry layer, we define the cohesion index ξ :

$$\xi = \frac{\sigma_c}{\sigma_p} = \frac{2\pi\gamma_s \cos(\Theta_\ell)}{\rho\phi gh d \cos\theta}, \quad (6)$$

where h is the height of the non-cohesive medium, ρ the particle density, and ϕ the solid volume fraction.

The non-cohesive layer is assumed to be in a flow state. At the interface, the ratio of shear stress to normal stress is governed by the inertial number I , defined as $I = \sqrt{\sigma_k/\sigma_p}$. The effective friction $\mu(I)$ of this layer is described by the $\mu(I)$ rheology [14]:

$$\mu(I) = \mu_0 + \frac{\mu_1 - \mu_0}{1 + I_0/I} \quad (7)$$

$$\simeq \mu_0(1 + \alpha I), \quad (8)$$

where

$$\alpha \simeq (\mu_1 - \mu_0)/(\mu_0 I_0). \quad (9)$$

While for a steady-state flow on an inclined plane $\mu(I) = \tan\theta$, we also consider transient regimes where I must be calculated from the local shear rate $\dot{\gamma}$ at the interface:

$$I = \sqrt{\frac{d^2 \dot{\gamma}^2}{\phi gh \cos\theta}}. \quad (10)$$

The transition from the slow erosion regime to the fast erosion regime occurs when the macroscopic stability limit of the cohesive bed is reached. This boundary is defined by the condition where the stress ratio exerted by the dry flow matches the cohesive yield threshold:

$$\mu(I) = \mu_c. \quad (11)$$

Substituting the linearized form of $\mu(I)$ from Eq. (8) and the definition of μ_c from Eq. (4), we obtain:

$$\mu_0(1 + \alpha I) = \mu_0(1 + a\xi), \quad (12)$$

which simplifies to a critical ratio between the inertial number and the cohesion index:

$$\frac{I}{\xi} = \frac{a}{\alpha}. \quad (13)$$

This stability criterion leads to two distinct physical scenarios:

- Slow Erosion ($I/\xi < a/\alpha$): The bed is macroscopically stable. Erosion occurs via stochastic, grain-by-grain detachment driven by velocity fluctuations within the dry flow.
- Fast Erosion ($I/\xi > a/\alpha$): The mean shear stress exceeds the bed's resistance, leading to a progressive failure of the cohesive layers.

By combining Eqs. (10) and (6), the condition Eq. (13) can be expressed as a critical inclination angle, provided the local shear rate $\dot{\gamma}$ is known. In the following sections, $\dot{\gamma}$ is determined from the velocity profiles within the non-cohesive layer.

B. Slow erosion regime

In the slow erosion regime, the stress ratio σ_τ/σ_p applied by the non-cohesive flow at the interface remains below the cohesive yield threshold μ_c defined in Eq. (4). Consequently, the cohesive bed is macroscopically stable and does not undergo global failure. However, at the particle scale, the interface is subjected to a continuous bombardment by the overlying dry grains. This bombardment can trigger individual detachment events through a stochastic process governed by the competition between the local bond energy E_b and the fluctuating kinetic energy e_k of the dry particles.

The energy required to rupture a cohesive bond can be scaled as $E_b \sim \sigma_c d^3$. Conversely, the mean kinetic energy of a grain in the dry flow, $\langle e_k \rangle$, is proportional to the kinetic stress σ_k :

$$\langle e_k \rangle \sim \sigma_k d^3 \sim \rho d^5 \dot{\gamma}^2, \quad (14)$$

In this regime, since the mean shear stress is insufficient to break the bed, the mean kinetic energy is typically lower than the bond energy ($\langle e_k \rangle < E_b$).

Under this sub-threshold condition, an erosion event can occur through kinetic energy fluctuations: the instantaneous velocity \mathbf{u} of a dry grain at the interface fluctuates due to collisions. In dense granular flows, the distribution of these fluctuations often exhibits high-energy tails. A detachment is triggered if an impacting grain belongs to this tail, such that its instantaneous kinetic energy $e_k = \frac{1}{2} m u^2$ exceeds E_b .

The probability of detachment P_{det} depends on the probability density function of the energy fluctuations $P(e_k)$. Assuming an exponential decay for the high-energy tails, as frequently observed in sheared granular media, the detachment probability can be modeled by an Arrhenius-like activation law:

$$P_{det} \propto \exp\left(-\beta \frac{E_b}{\langle e_k \rangle}\right) = \exp\left(-\beta \frac{\sigma_c}{\sigma_k}\right), \quad (15)$$

where β is a non-dimensional coefficient related to the flow microstructure and the efficiency of energy transfer. Hence, as long as the dry layer is in motion, P_{det} remains non-zero.

We define the surface erosion rate K_e as the interfacial detachment frequency:

$$K_e = \frac{1}{N_s} \frac{dN_e}{dt} \quad (16)$$

where N_s is the number of particles currently exposed at the wet-dry interface. K_e can be estimated by the frequency of interface attempts $f \sim \dot{\gamma}$ over the number of particle sites multiplied by the detachment probability:

$$K_e \sim \dot{\gamma} \exp\left(-\beta \frac{2\pi\gamma_s \cos \Theta_\ell}{\rho d^3 \dot{\gamma}^2}\right). \quad (17)$$

In summary, the slow regime is characterized by a frequency-dependent, thermally-activated-like process where the erosion rate is extremely sensitive to the ratio σ_c/σ_k .

C. Fast erosion regime

When the stress ratio at the interface exceeds the cohesive yield threshold ($I/\xi > a/\alpha$), the system enters the fast erosion regime. Unlike the stochastic process described in the previous section, this regime is characterized by a global mechanical instability of the interface. In this state, the mean shear stress exerted by the flowing dry layer is sufficient to overcome the macroscopic resistance of the cohesive bed. Consequently, erosion is no longer limited to rare, intermittent events but involves in addition a continuous and correlated failure of the cohesive layers.

In the fast regime, the mean-field driving forces (pressure σ_p and shear stress σ_τ) dominate the local bonding forces. While statistical fluctuations in the particle velocities still exist, they no longer play a leading role because the *average* energy transfer from the dry flow to the bed is sufficient to trigger detachment. The process remains fundamentally interfacial, but it manifests itself as a progressive destabilization where the shear from the non-cohesive flow penetrates the cohesive bed, effectively entraining particles in a collective manner.

A defining feature of this regime is its characteristic timescale, τ_f , which is expected to be significantly shorter than the long waiting times associated with the activated

detachment in the slow regime. To estimate τ_f , we consider the dynamics of a non cohesive particle of mass $m \sim \rho d^3$ located at the interface. Under the action of the mean confining pressure σ_p , the particle is subjected to a characteristic force $F_p \sim \sigma_p d^2$. We define τ_f as the time required for this force to accelerate the particle until it acquires a kinetic energy equal to the cohesive bond energy, $E_b \sim \sigma_c d^3$. Following the second law of motion, we have $F_p \cdot \tau_f \sim m \cdot v$, where v is the velocity such that $\frac{1}{2}mv^2 \sim \sigma_c d^3$. This yields $v \sim \sqrt{\sigma_c/\rho}$. Substituting this into the momentum balance, we obtain

$$\tau_f \sim \frac{mv}{F_p} \sim \frac{(\rho d^3)\sqrt{\sigma_c/\rho}}{\sigma_p d^2} = \frac{d\sqrt{\rho\sigma_c}}{\sigma_p}. \quad (18)$$

By introducing the dimensionless numbers $I = \dot{\gamma}d/\sqrt{\sigma_p/\rho}$ and $\xi = \sigma_c/\sigma_p$, this timescale can be rewritten in terms of the macroscopic flow parameters:

$$\tau_f \sim \frac{I\sqrt{\xi}}{\dot{\gamma}}. \quad (19)$$

The derivation of τ_f suggests that the surface erosion rate in this regime, K_e (Eq. (16)), scales with the inverse of this characteristic time. Since the onset of this regime is governed by the ratio I/ξ , we expect the erosion rate to be a function of this parameter:

$$K_e \propto \tau_f \mathcal{F}\left(\frac{I}{\xi}\right) = \frac{\dot{\gamma}}{d^2 I \sqrt{\xi}} \mathcal{F}\left(\frac{I}{\xi}\right), \quad (20)$$

where \mathcal{F} is a scaling function to be determined.

While this mean-field analysis provides the governing scales of the problem, the complex spatial and temporal evolution of the interface during mass entrainment—particularly the feedback between the increasing thickness of the dry layer and the erosion of the bed—requires a more detailed investigation. In the following sections, we explore the functional form of \mathcal{F} from DEM simulations to characterize the evolution of the erosion rate across a wide range of system parameters.

III. NUMERICAL PROCEDURES

A. Simulation method

Numerical simulations are performed using an in-house software, cFGd3D [36, 37], which is based on the DEM [38–41]. This method falls under the broader category of particle dynamics techniques, similar to molecular dynamics used for simulating molecular systems [42] and contact dynamics (CD) used to model systems with frictional contacts [43–45].

In the basic DEM framework, particles interact via local force laws [46], with these forces depending on contact strains, which are determined in terms of the relative displacements of the particles. The code implements a velocity-Verlet scheme [42] for step-wise integration of

Newton's second law equations of motion for spherical particles.

The total interaction force \mathbf{f} between two particles consists of normal and tangential components f_n and \mathbf{f}_t , respectively:

$$\mathbf{f} = f_n \mathbf{n} + \mathbf{f}_t, \quad (21)$$

where \mathbf{n} is the contact normal. The normal force f_n is the sum of the visco-elastic force f_{ed} and the capillary force f_{cap} :

$$f_n = f_{ed} + f_{cap}. \quad (22)$$

The distance δ_n represents elastic deflection (negative for overlap) or capillary bond length (positive for gap). The visco-elastic force f_{ed} is the sum of linear elastic repulsion $f_n^e = -k_n \delta_n$ and viscous damping $f_n^d = -\gamma_n \dot{\delta}_n$, where γ_n is the damping coefficient. The total normal force f_{ed} is given by:

$$f_{ed} = \begin{cases} -k_n \delta_n - \gamma_n \dot{\delta}_n & \text{if } f_{ed} > 0 \text{ and } \delta_n \leq 0, \\ 0 & \text{otherwise.} \end{cases} \quad (23)$$

This ensures that f_{ed} remains positive for dry contacts, but may become negative (attractive) when capillary forces are considered.

The liquid is assumed to be in the pendular state, where small liquid bridges join particles. The capillary stress increases with the amount of liquid in this state [11], while it remains nearly constant in the funicular state [47, 48]. We model the capillary interaction as a binary force law, which provides a good approximation even at higher liquid volumes.

Capillary bonds are persistent and reversible unless the gap distance exceeds a rupture distance d_{rupt} , beyond which the liquid bridge collapses. The rupture distance depends on the bond volume V_b and is given by:

$$d_{rupt} = \left(1 + \frac{\theta_\ell}{2}\right) V_b^{1/3}, \quad (24)$$

where θ_ℓ is the particle-liquid-gas contact angle. This assumption simplifies DEM simulations, avoiding complex thermodynamic or hydrodynamic considerations [12, 49].

The capillary force f_{cap} is derived from the Young-Laplace equation [50], approximated as:

$$f_{cap} = \begin{cases} -\pi d \gamma_s \cos \theta_\ell & \text{for } \delta_n < 0, \\ -\pi d \gamma_s \cos \theta_\ell e^{-\delta_n/\lambda} & \text{for } 0 \leq \delta_n \leq d_{rupt}, \end{cases} \quad (25)$$

where $\lambda \simeq 0.9 \left(\frac{2V_b}{d}\right)^{1/2}$.

For tangential forces, we use a linear elastic law with Coulomb friction:

$$\mathbf{f}_t = \begin{cases} -k_t \boldsymbol{\delta}_t - \gamma_t \dot{\boldsymbol{\delta}}_t & \text{if } \|\mathbf{f}_t\| \leq \mu_p f_n^e, \\ -\mu_p f_n^e \frac{\dot{\boldsymbol{\delta}}_t}{\|\dot{\boldsymbol{\delta}}_t\|} & \text{otherwise,} \end{cases} \quad (26)$$

where μ_p is the friction coefficient, k_t is the tangential stiffness, and γ_t is the tangential damping parameter. $\boldsymbol{\delta}_t$ is the cumulative tangential displacement, and $\dot{\boldsymbol{\delta}}_t$ is the relative tangential velocity.

TABLE I: Simulation parameters

Description	Value
Number of particles, N_p	8,000
Particle diameter, d	3×10^{-4} m
Particle density, ρ	2.5 g cm^{-3}
Normal stiffness, k_n	$1 \times 10^2 \text{ N m}^{-1}$
Normal damping, γ_n	$3 \times 10^{-3} \text{ N s m}^{-1}$
Tangential stiffness, k_t	$8 \times 10^1 \text{ N m}^{-1}$
Tangential damping, γ_t	$3 \times 10^{-3} \text{ N s m}^{-1}$
Friction coefficient, μ_p	0.5
Contact angle, Θ_ℓ	5°
Time step, dt	1×10^{-6} s
De-bonding distance, d_{rupt}	3×10^{-5} m
Inclination angle, θ	$[25^\circ - 32^\circ]$
Liquid surface tension, γ_s	$[8 \times 10^{-3} \text{ N m}^{-1} - 4 \times 10^{-2} \text{ N m}^{-1}]$

B. System preparation

The granular bed is composed of $N_p = 8,000$ non-cohesive monodisperse spherical particles with a diameter $d = 3 \times 10^{-4}$ m and a density $\rho = 2500 \text{ kg m}^{-3}$. The particles are dropped into a rectangular domain under the effect of gravity. The domain has dimensions of length $L_x = 26d$, width $L_y = 10d$, and height $L_z = 28d$. Once the particles reach their equilibrium state, the lateral walls are removed and we apply periodic boundary conditions along the x and y directions.

The simulated system is divided into three layers, as illustrated in Fig. 2: a rough fixed base at the bottom of the sample, consisting of densely packed particles with a height nearly $3d$ to prevent sliding (grey layer), a cohesive layer of thickness $12d$ (3,500 wet particles in red), and non-cohesive layer of thickness $13d$ (4000 dry particles in blue). The cohesive forces are activated between particles that belong to the cohesive layer and are separated by a distance less than or equal to the debonding distance $d_{rupt} = 0.1d$. This ensures a uniform distribution of the wetting fluid on all particles.

In this work, we assume irreversible breakage of capillary bonds to ensure that the eroded layer is not regenerated again. Indeed, in a large system of particles, once a particle gets eroded away from the wet layer, the liquid it carries is rapidly dispersed by the flow so that the particle becomes dry. This assumption implies an irreversible extraction of particles from the wet layer. In the simulations, the status of a particle which has lost all its capillary bonds is changed from ‘‘wet’’ to ‘‘dry’’. The debonding distance in all simulations is set to $d_{rupt} = 0.1d$. Note also that the interactions between wet and dry particles are assumed to be noncohesive. In other words, the capillary bonds are effective only between wet particles.

The system is tilted by rotating the gravity vector of coordinates $(g \sin(\theta), 0, g \cos(\theta))$. We vary the inclination angle θ and liquid surface tension γ_s in the cohesive layer. The ranges of values of these parameters and all constant system parameters used in this study are summarized in Table I.

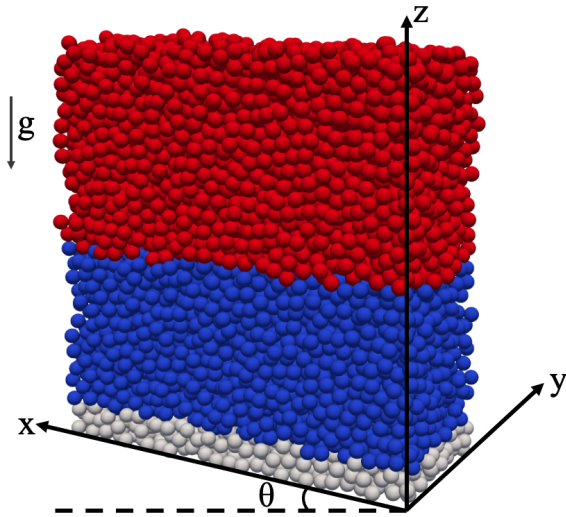


FIG. 2: A snapshot of the granular bed in its initial configuration, consisting of 3,500 wet particles (blue) overlaid by a non-cohesive bed of 4,000 dry particles (red). Additionally, 1000 immobile particles are stuck to the bottom of the sample (grey). The gravity vector is rotated to an angle θ (above the angle of repose) to trigger the flow of the particles in the non-cohesive layer.

IV. SIMULATION RESULTS

A. Phenomenology

The erosion process is a consequence of the irreversible rupture of capillary bonds at the interface between the wet and dry layers. This is illustrated in Fig. 3, providing a typical example of the system's evolution from its initial tilting at time $t = 0$ to the completion of the erosion. The cohesive bed of initially wet particles, indicated by blue particles in Fig. 3, is placed at the bottom, just above a rough, immobile base represented by gray grains. In these snapshots the particles keep their initial color. For this reason, the blue eroded particles, which are dispersed inside the dry layer, are no more wet.

The inclination angle θ is chosen to be larger than the avalanche angle θ_0^d (with $\tan \theta_0^d = \mu_0$) of the non-cohesive dry medium but smaller than the avalanche angle θ_0^w (with $\tan \theta_0^w = \mu_c$) of the wet cohesive layer. As a result, the cohesive bed does not flow while the non-cohesive layer flows over it. The interface between the two layers is the locus of erosion where wet particles are gradually detached and carried away by the dry flow. Consequently, the cohesive phase thins over time while eroded particles spread evenly into the non-cohesive region, causing the thickness of the non-cohesive layer to increase. This behavior is observed across a broad range of the values of the liquid surface tension and tilt angle.

Fig. 4 shows velocity profiles at several instants during the erosion of a wet bed. These profiles are calculated by averaging the particle velocities within layers parallel to

the slope, each with a thickness of $\delta z = d$, where d is the particle diameter. The average velocity is calculated over a time interval δt that is much shorter than the system's characteristic evolution time. Only the x -component of the velocity (along the inclined plane) has a non-zero average, as shown in Fig. 4. Initially, the velocity profile is zero, as the system starts at rest. As the erosion proceeds, the velocity profile splits into two distinct zones. The first zone, at the bottom of the sample, corresponds to the cohesive bed where the velocity is zero. Note that particle velocities within the rough base are fixed at zero and are not shown ($z < 0$). Above a certain height, the average particle velocity becomes non-zero. This height marks the separation interface between the cohesive and non-cohesive parts, which evolves over time. Initially, this interface is at the midpoint of the system but gradually moves downward as the erosion process continues, eventually reaching zero when the process is complete.

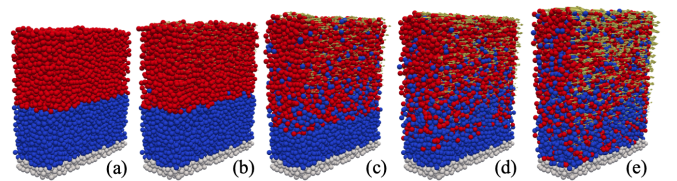


FIG. 3: Snapshots showing the time evolution of the erosion process for an inclination angle $\theta = 32^\circ$. Velocity vector thickness is proportional to particle velocity. Time snapshots: (a) $t = 0.1$ s, (b) $t = 0.5$ s, (c) $t = 8$ s, (d) $t = 10$ s, and (e) $t = 13$ s. The corresponding velocity profiles are shown in Fig. 4. In these snapshots, the particles keep their initial color as shown in Fig. 2 although the blue eroded particles (dispersed inside the dry layer) are no more wet.

As an illustration, Figs. 6 and 5 display the evolution of the total number N_e of eroded particles as a function of time for various values of the surface tension and inclination angle. Since the erosion process takes place at the interface between the cohesive and non-cohesive regions, we normalize N_e by the average number N_s of particles at the interface. The latter remains constant during the process. Significant differences are observed between the results presented in Fig. 5 and those in Fig. 6. Fig. 5 characterizes the slow erosion regime, whereas the curves in Fig. 6 correspond to the fast erosion regime, as it will be discussed in detail in Section IV B. For a given erosion duration, the values of the normalized number of eroded particles, N_e/N_s , are several orders of magnitude lower in Fig. 5 than in Fig. 6. The discrete “staircase” jumps visible in Fig. 5 correspond, at their smallest scale, to the detachment of single particles. In some instances, the jump amplitude is an integer multiple of this fundamental unit, suggesting that the removal of a single grain can locally destabilize neighboring particles.

In the present study, we do not focus extensively on the slow erosion regime. Simulating this regime poses a significant numerical challenge due to the vast separation

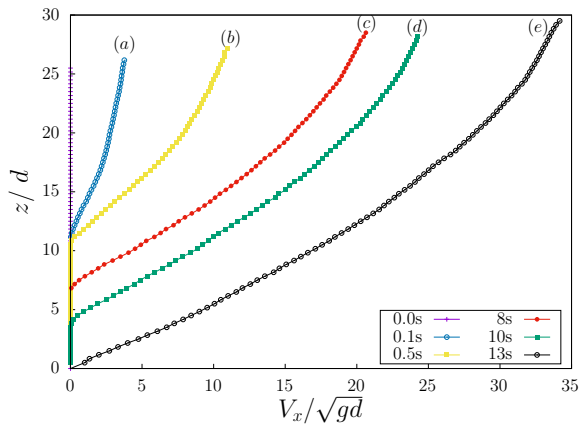


FIG. 4: Normalized velocity profiles, using the characteristic velocity \sqrt{gd} , along the direction of flow as a function of normalized height z/d for a system of surface tension $\gamma_s = 0.03 \text{ N m}^{-1}$ and inclination angle $\theta = 32^\circ$ at several instants of time corresponding to the snapshots (a-e) in Fig. 3. The flow is initially at rest ($t = 0 \text{ s}$), with the dry system beginning to flow while the velocity in the cohesive bed remains zero. As erosion progresses, the thickness of the static wet layer decreases. In the final stage, the entire sample flows as the cohesive layer becomes fully eroded.

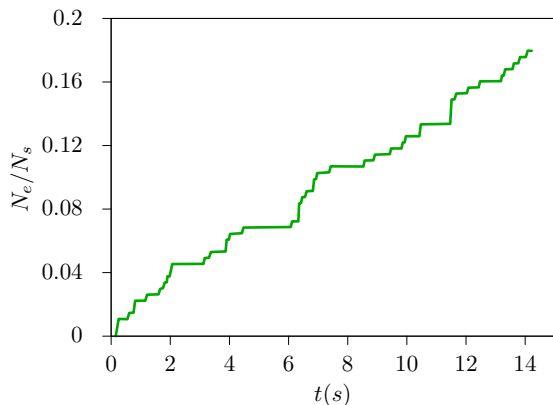


FIG. 5: Temporal evolution of the number of eroded particles N_e , normalized by the average number of particles N_s located at the interface between the cohesive and non-cohesive zones. The data are obtained from DEM simulations with a surface tension $\gamma_s = 0.03 \text{ N/m}$ and an inclination angle $\theta = 25^\circ$.

of timescales between the fast particle dynamics within the non-cohesive flow and the extremely low frequency of erosion events. A systematic investigation of the slow erosion regime will be the subject of a future publication. Nevertheless, the data in Fig. 5 allow for a preliminary estimation of the dimensionless coefficient β introduced in Eq. (17). Analysis of the velocity profiles within the dry flow provides the local shear rate at the interface, $\dot{\gamma} \approx 70 \text{ s}^{-1}$ for the case shown in Fig. 5. Substituting this value into Eq. (17) yields an estimate of $\beta \approx 0.015$.

We now shift our focus to the fast erosion regime. Our

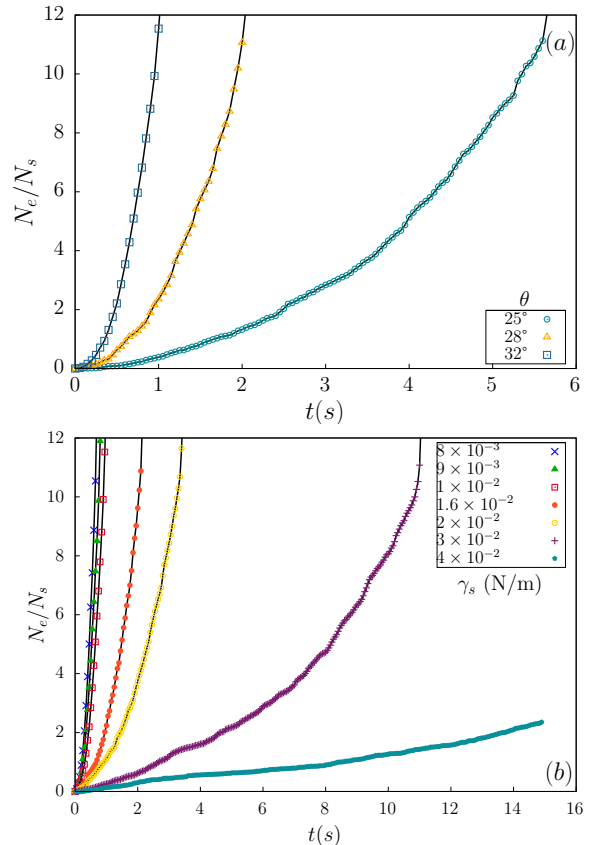


FIG. 6: Time evolution of the number N_e of eroded particles normalized by the average number N_s of particles at the interface between the cohesive and non-cohesive zones. (a) For three values of the inclination angle θ with $\gamma = 0.01 \text{ N m}^{-1}$, and (b) different values of the liquid surface tension with $\theta = 32^\circ$.

objective is to determine the functional form of \mathcal{F} , which allows for the calculation of the surface erosion rate K_e as a function of the dimensionless group I/ξ and the characteristic timescale $\tau_f = I\sqrt{\xi}/\dot{\gamma}$.

B. Analysis in the fast erosion regime

Figure 6 indicates that the number of eroded particles follows a nonlinear evolution over time, with a rate that increases sharply with the inclination angle. This nonlinear progression of $N_e(t)$ is primarily attributed to the evolving height h of the non-cohesive layer. As erosion proceeds, the increasing thickness of the dry layer modifies both the confining pressure σ_p and the local shear rate $\dot{\gamma}$ at the interface, thereby creating a feedback loop in the erosion dynamics.

The evolution of the normalized number of eroded particles, $N_e(t)/N_s$, is detailed in Fig. 6(a) for a surface tension $\gamma_s = 0.01 \text{ mN/m}$ at three distinct inclination angles ($\theta = 25^\circ, 28^\circ$, and 32°). Conversely, Fig. 6(b) presents the evolution of $N_e(t)/N_s$ at a fixed inclination of $\theta = 32^\circ$

for surface tension values ranging from $\gamma_s = 8 \times 10^{-3}$ N/m to 4×10^{-2} N/m. Consistent with physical expectations, the erosion rate is enhanced by both steeper inclination angles and reduced surface tension.

For each combination of surface tension γ_s and inclination angle θ , and at every time step during the erosion process, we extract the surface erosion rate K_e from the data in Fig. 6. The instantaneous height h and the corresponding shear rate $\dot{\gamma}$ at the wet-dry interface are simultaneously determined from the velocity profiles as those shown in Fig. 4.

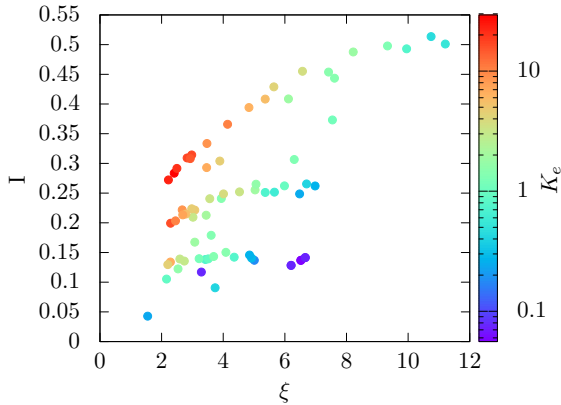


FIG. 7: Dimensionless mapping of the surface erosion rate $K_e = \frac{1}{N_s} \frac{dN_e}{dt}$ as a function of the interfacial inertial number I and the cohesion index ξ . The data set comprises results from simulations spanning surface tensions γ_s from 8×10^{-3} N/m to 4×10^{-2} N/m and inclination angles θ between 25° and 32° . The color scale represents the magnitude of the erosion rate, illustrating the transition between different erosion intensities within the I - ξ parameter space.

Fig. 7 presents a comprehensive mapping of the inertial number I , the cohesion index ξ , and the resulting surface erosion rate K_e (indicated by the color scale) for the entire set of simulations. The data points aggregated in this plot encompass the full range of inclination angles θ and surface tension values γ_s investigated, captured at successive temporal intervals throughout each simulation.

Following the scaling arguments developed in Eq. (20), we examine the relationship between the surface erosion rate and the dimensionless control parameters. By plotting the product of the erosion rate and the characteristic timescale, $\tau_f K_e = \frac{I\sqrt{\xi}}{\dot{\gamma}} K_e$, as a function of the ratio I/ξ , we observe that all data points nicely collapse onto a single master curve, as shown in Fig. 8. This collapse, which holds across the entire range of investigated inclination angles and surface tension values in the fast erosion regime, confirms that I/ξ is the fundamental dimensionless group governing the transition to and the intensity of the fast erosion regime.

The master curve is accurately described by a power-

law relationship of the form:

$$\frac{I\sqrt{\xi}}{\dot{\gamma}} K_e = A \left[\frac{I}{\xi} - \left(\frac{I}{\xi} \right)^* \right]^\kappa, \quad (27)$$

where the best-fit parameters are found to be $\kappa \simeq 1.97$, $A \simeq 6$, and a critical threshold $(I/\xi)^* \simeq 0.02$.

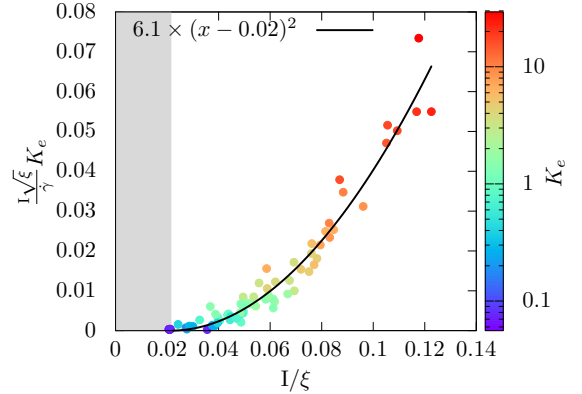


FIG. 8: Reduced erosion rate $\frac{I\sqrt{\xi}}{\dot{\gamma}} K_e$ as a function of I/ξ . The solid curve is the result of a fit of the form $\frac{I\sqrt{\xi}}{\dot{\gamma}} K_e = A[(I/\xi) - (I/\xi)^*]^\kappa$, with $\kappa = 1.97$, $A = 6$ and $(I/\xi)^* = 0.02$.

The near-quadratic exponent ($\kappa \approx 2$) suggests a significant non-linear sensitivity of the erosion rate to the excess stress ratio.

To evaluate the consistency of our results, we compare the threshold value $(I/\xi)^*$ obtained from the numerical fit with the theoretical prediction a/α derived from Eq. (13). Following the methodology of Vo et al. [24], we adopt $a = 0.095$. The parameter α is estimated using the standard rheological values for hard spheres with an inter-particle friction coefficient $\mu_p = 0.5$ [14]. Taking the values $I_0 \approx 0.3$, $\mu_0 \approx 0.4$, and $\mu_1 \approx 1.0$, we calculate $\alpha = (\mu_1 - \mu_0)/(\mu_0 I_0) \approx 5$. This leads to a theoretical ratio $a/\alpha \approx 0.019$. This value is in agreement with the threshold $(I/\xi)^* \simeq 0.02$ determined from our data collapse.

It should be noted that certain physical parameters, such as the particle diameter d , density ρ , and gravitational acceleration g , were held constant throughout this study. Furthermore, the established relationships were obtained for fixed values of the capillary bridge rupture distance and the wetting angle. A complementary investigation exploring the influence of these additional parameters would be of significant value to further generalize these findings.

By substituting the definitions of the inertial number and cohesion index, the threshold for the fast erosion regime can be reformulated directly in terms of the mechanical stresses. Specifically, the condition for the onset of fast erosion becomes:

$$\sqrt{\sigma_k \sigma_p} \geq b \sigma_c, \quad (28)$$

where $b = (I/\xi)^* \simeq 0.02$. This expression highlights the fundamental interplay between the destabilizing stresses—the kinetic stress σ_k and the confining pressure σ_p —and the resisting cohesive strength σ_c . Equation (28) reveals that the erosion threshold is governed by the ratio of the geometric mean of the driving stresses to the cohesive resistance. Remarkably, this suggests that the kinetic and confining stresses contribute with equal weight to the destabilization of the interface. This criterion can also be viewed as a limit on the sustainable cohesion for a given flow state:

$$\sigma_c \leq \frac{I\sigma_p}{b}. \quad (29)$$

Furthermore, by introducing the effective friction coefficient $\mu(I) = \sigma_\tau/\sigma_p$, where σ_τ is the shear stress at the interface, the erosion condition can be expressed as a function of the tangential loading:

$$\sigma_\tau \geq \frac{b\mu(I)\sigma_c}{I}. \quad (30)$$

This formulation underscores the role of shear stress in the erosion process. More importantly, Eq. (30) demonstrates that a simple comparison between shear stress and cohesive strength is insufficient to characterize the erosion threshold; the dynamical state of the flow, encapsulated by the inertial number I , must also be explicitly considered to account for the mechanical stability of the interface.

V. CONCLUSION

In this study, we have employed DEM simulations to investigate the microscopic mechanisms governing the erosion of a cohesive granular bed subjected to the shear flow of a non-cohesive dry layer. By modeling interparticle cohesion through capillary bridge forces, we characterized erosion as the irreversible rupture of these liquid bonds at the interface. Our results reveal that the transition from stability to entrainment is not merely a function of a single stress threshold, but involves rather a complex interplay between the dynamical state of the dry flow and the mechanical resistance of the wet bed.

A key contribution of this work is the identification of two distinct erosion regimes: the first regime is a slow, stochastic regime where the mean driving stresses are below the yield threshold. In this case, we hypothesized that erosion is activated by high-energy fluctuations in the granular temperature of the dry flow, following an Arrhenius-like probability law. The second regime is a fast, collective regime characterized by a mean-field mechanical instability of the interface.

Through systematic variations of the inclination angle and surface tension, we demonstrated that the surface erosion rate K_e in the fast erosion regime is governed by a robust scaling law. By introducing a characteristic timescale τ_f derived from the competition between confining pressure and cohesive energy, we achieved a remarkable data collapse. This collapse highlights that the ratio of the inertial number I to the cohesion index ξ is the fundamental dimensionless group controlling the process. Our findings, summarized by the condition $\sqrt{\sigma_k\sigma_p} \geq b\sigma_c$, prove that the geometric mean of the kinetic and confining stresses must overcome the cohesive strength to initiate rapid erosion. This result underscores that shear stress alone is insufficient to characterize the erosion threshold; the dynamical inertia of the flow must be explicitly accounted for.

While our model provides a clear scaling framework by neglecting liquid viscosity, it serves as a baseline for more complex fluid-grain interactions. The scaling laws established here offer a predictive tool for broader contexts where cohesive media are eroded by granular flows, including industrial transport and geophysical events where driving forces may stem from sources other than gravity.

Future research should aim to extend this framework by incorporating lubrication forces and viscous effects within the capillary bridges. Such additions would be essential for capturing regimes where high shear rates or high liquid viscosities make viscous dissipation comparable to capillary attraction. Furthermore, exploring the reversibility of capillary bonds—allowing for the re-agglomeration of eroded particles—could provide a more nuanced understanding of mass balance in closed granular systems.

-
- [1] Stephan Herminghaus. Dynamics of wet granular matter. *Advances in physics*, 54(3):221–261, 2005.
- [2] Namiko Mitarai and Franco Nori. Wet granular materials. *Advances in physics*, 55(1-2):1–45, 2006.
- [3] Thanh-Trung Vo, Patrick Mutabaruka, Saeid Nezamabadi, Jean-Yves Delenne, and Farhang Radjai. Evolution of wet agglomerates inside inertial shear flow of dry granular materials. *Physical Review E*, 101(3):032906, 2020.
- [4] Gautier Lefebvre and Pierre Jop. Erosion dynamics of a wet granular medium. *Phys. Rev. E*, 88:032205, Sep 2013.
- [5] Farhang Radjai, Vincent Topin, Vincent Richefeu, Charles Voivret, Jean-Yves Delenne, Emilien Azéma, and Said El Youssoufi. Force transmission in cohesive granular media. In *AIP Conference Proceedings*, volume 1227, pages 240–259. American Institute of Physics, 2010.
- [6] Ralph Alger Bagnold. Experiments on a gravity-free dispersion of large solid spheres in a newtonian fluid under shear. *Proceedings of the Royal Society of London. Series*

- A. Mathematical and Physical Sciences*, 225(1160):49–63, 1954.
- [7] Frédéric Da Cruz, Sacha Emam, Michaël Prochnow, Jean-Noël Roux, and François Chevoir. Rheophysics of dense granular materials: Discrete simulation of plane shear flows. *Physical Review E*, 72(2):021309, 2005.
- [8] Simon M Iveson, Jai A Beathé, and Neil W Page. The dynamic strength of partially saturated powder compacts: the effect of liquid properties. *Powder Technology*, 127(2):149–161, 2002.
- [9] Peder CF Møller and D Bonn. The shear modulus of wet granular matter. *Europhysics Letters*, 80(3):38002, 2007.
- [10] PG Rognon, J-N Roux, D Wolf, M Naaïm, and F Chevoir. Rheophysics of cohesive granular materials. *Europhysics Letters*, 74(4):644, 2006.
- [11] Vincent Richefeu, Moulay Saïd El Youssofi, and Farhang Radjai. Shear strength properties of wet granular materials. *Physical Review E*, 73(5):051304, 2006.
- [12] Lama Braysh, Patrick Mutabaruka, Farhang Radjai, and Serge Mora. Dynamics of wet granular flows down an inclined plane. *Journal of Rheology*, 69:409–422, 2025.
- [13] GDR-MiDi. On dense granular flows. *Eur. Phys. J. E*, 14:341–365, 2004.
- [14] Pierre Jop, Yoël Forterre, and Olivier Pouliquen. A constitutive law for dense granular flows. *Nature*, 441(7094):727–730, Jun 2006.
- [15] Ken Kamrin and Georg Koval. Nonlocal constitutive relation for steady granular flow. *Physical review letters*, 108(17):178301, 2012.
- [16] Nicolas Berger, Emilien Azéma, Jean-François Douce, and Farhang Radjai. Scaling behaviour of cohesive granular flows. *Europhysics Letters*, 112(6):64004, 2016.
- [17] Saeed Khamseh, Jean-Noël Roux, and François Chevoir. Flow of wet granular materials: A numerical study. *Physical Review E*, 92(2):022201, 2015.
- [18] M Badetti, A Fall, D Hautemayou, F Chevoir, Patrick Aïmedieu, S Rodts, and J-N Roux. Rheology and microstructure of unsaturated wet granular materials: Experiments and simulations. *Journal of rheology*, 62(5):1175–1186, 2018.
- [19] Olivier Pouliquen, Cyril Cassar, Pierre Jop, Yoël Forterre, and Maxime Nicolas. Flow of dense granular material: towards simple constitutive laws. *Journal of Statistical Mechanics: Theory and Experiment*, 2006(07):P07020, 2006.
- [20] Yoël Forterre and Olivier Pouliquen. Flows of dense granular media. *Annu. Rev. Fluid Mech.*, 40:1–24, 2008.
- [21] Michel Badetti, Abdoulaye Fall, François Chevoir, and Jean-Noël Roux. Shear strength of wet granular materials: Macroscopic cohesion and effective stress: Discrete numerical simulations, confronted to experimental measurements. *The European Physical Journal E*, 41:1–16, 2018.
- [22] François Boyer, Élisabeth Guazzelli, and Olivier Pouliquen. Unifying suspension and granular rheology. *Physical review letters*, 107(18):188301, 2011.
- [23] Martin Trulsson, Bruno Andreotti, and Philippe Claudin. Transition from the viscous to inertial regime in dense suspensions. *Physical review letters*, 109(11):118305, 2012.
- [24] Thanh Trung Vo, Saeid Nezamabadi, Patrick Mutabaruka, Jean-Yves Delenne, and Farhang Radjai. Additive rheology of complex granular flows. *Nature communications*, 11(1):1476, 2020.
- [25] Thanh-Trung Vo. Erosion dynamics of wet particle agglomerates. *Computational Particle Mechanics*, 8(3):601–612, 2021.
- [26] Lhassan Amarsid, J-Y Delenne, Patrick Mutabaruka, Yann Monerie, Frédéric Perales, and Farhang Radjai. Viscoinertial regime of immersed granular flows. *Physical Review E*, 96(1):012901, 2017.
- [27] Franco Tapia, Mie Ichihara, Olivier Pouliquen, and Élisabeth Guazzelli. Viscous to inertial transition in dense granular suspension. *Phys. Rev. Lett.*, 129:078001, Aug 2022.
- [28] A Hassanpour, SJ Antony, and M Ghadiri. Effect of size ratio on the behaviour of agglomerates embedded in a bed of particles subjected to shearing: Dem analysis. *Chemical engineering science*, 62(4):935–942, 2007.
- [29] Ali Hassanpour, S Joseph Antony, and Mojtaba Ghadiri. Modeling of agglomerate behavior under shear deformation: effect of velocity field of a high shear mixer granulator on the structure of agglomerates. *Advanced Powder Technology*, 18(6):803–811, 2007.
- [30] A Mangeney, Olivier Roche, O Hungr, N Mangold, Gloria Faccanoni, and A Lucas. Erosion and mobility in granular collapse over sloping beds. *Journal of Geophysical Research: Earth Surface*, 115(F3), 2010.
- [31] Xurong He, Xiewen Hu, Zihao Huo, Jianfeng Tang, and Shilin Zhang. Study on dynamic mechanism of granular flow erosion and entrainment based on dem theory. *Geoenviron Disasters*, 11:1–13, article no. 17, 2024.
- [32] Eric Lajeunesse, Luce Malverti, and François Charru. Bed load transport in turbulent flow at the grain scale: Experiments and modeling. *Journal of Geophysical Research: Earth Surface*, 115(F4), 2010.
- [33] François Charru, Héléne Mouilleron, and Olivier Eiff. Erosion and deposition of particles on a bed sheared by a viscous flow. *Journal of Fluid Mechanics*, 519:55–80, 2004.
- [34] Bryan J Ennis, Gabriel Tardos, and Robert Pfeffer. A microlevel-based characterization of granulation phenomena. *Powder Technology*, 65(1-3):257–272, 1991.
- [35] Mohammadreza Alizadeh Behjani, Nejat Rahmanian, Ali Hassanpour, et al. An investigation on process of seeded granulation in a continuous drum granulator using dem. *Advanced Powder Technology*, 28(10):2456–2464, 2017.
- [36] Patrick Mutabaruka, Jean-Yves Delenne, Kenichi Soga, and Farhang Radjai. Initiation of immersed granular avalanches. *Phys. Rev. E*, 89:052203, May 2014.
- [37] Patrick Mutabaruka, Mahdi Taiebat, Roland J.-M. Pellenq, and Farhang Radjai. Effects of size polydispersity on random close-packed configurations of spherical particles. *Phys. Rev. E*, 100:042906, Oct 2019.
- [38] Peter A Cundall and Otto DL Strack. A discrete numerical model for granular assemblies. *geotechnique*, 29(1):47–65, 1979.
- [39] HJ Herrmann and Stefan Luding. Modeling granular media on the computer. *Continuum Mechanics and Thermodynamics*, 10:189–231, 1998.
- [40] C Thornton and SJ Antony. Quasi-static shear deformation of a soft particle system. *Powder technology*, 109(1-3):179–191, 2000.
- [41] Farhang Radjai and Frédéric Dubois, editors. *Discrete-element modeling of granular materials*. Iste-Wiley, New-York, March 2011. ISBN: 978-1-84821-260-2.
- [42] Michael P Allen, Dominic J Tildesley, et al. Computer

- simulation of liquids. *Clarendon-0.12*, 1987.
- [43] Jean Jacques Moreau. Some numerical methods in multi-body dynamics: application to granular materials. *European Journal of Mechanics-A/Solids*, 13(4-suppl):93–114, 1994.
 - [44] Farhang Radjai and Vincent Richefeu. Contact dynamics as a nonsmooth discrete element method. *Mechanics of Materials*, 41(6):715–728, 2009.
 - [45] Farhang Radjai. Multi-periodic boundary conditions and the contact dynamics method. *Comptes Rendus Mécanique*, 346(3):263–277, 2018.
 - [46] Hans J Herrmann, J-P Hovi, and S Luding. *Physics of dry granular media*, volume 350. Springer Science & Business Media, 2013.
 - [47] Mario Scheel, Ralf Seemann, Martin Brinkmann, Marco Di Michiel, Adrian Sheppard, and Stephan Herminghaus. Liquid distribution and cohesion in wet granular assemblies beyond the capillary bridge regime. *Journal of Physics: Condensed Matter*, 20(49):494236, 2008.
 - [48] Jean-Yves Delenne, Vincent Richefeu, and Farhang Radjai. Liquid clustering and capillary pressure in granular media. *Journal of Fluid Mechanics*, 762(R5):R5, 2015.
 - [49] Lama Braysh, Patrick Mutabaruka, Farhang Radjai, and Serge Mora. Breakage dynamics and scaling of wet aggregates of rigid particles. *Journal of Fluid Mechanics*, 1000:A39, 2024.
 - [50] T. Mikami, H. Kamiya, and M. Horio. Numerical simulation of cohesive powder behavior in fluidized bed. *Chemical Engineering Science*, 53(10):1927–1940, 1998.